Aqueous Photocatalytic Glycerol Oxidation to Formic Acid Coupled to H₂O₂ Production with an Anthraquinone Dye

Elena Tacchi, Greta Rossi, Mirco Natali,* Luka Đorđević,* and Andrea Sartorel*

The photocatalytic oxidation of glycerol into formic acid (FA) is reported employing a 9,10-anthraquinone-2,6-disulphonate disodium salt (AQDS) photocatalyst. The system operates in water, in the absence of additives, using O_2 as the oxidant and irradiating with blue light (λ = 415 nm). In 22 h, conversion of glycerol up to 79% leads to 30% yield of FA (turnover number of 15 for AQDS), with 79% selectivity among the products in solution and a quantum yield of 1.2%. The oxidation of glycerol is coupled to the reduction of oxygen to hydrogen peroxide (up to 16$\pm$5 mM), a high-added value photosynthetic product. A mechanistic investigation combining electron paramagnetic resonance (EPR) spectroscopy, transient absorption spectroscopy (TAS), and time-dependent density-functional theory (TD-DFT) calculations reveals a photoinduced hydrogen atom abstraction involving the triplet excited state ^{3*}AQDS and the glycerol substrate (k = 1.02($\pm$0.03)$\times 10^7$ M$^{-1}\cdot$s^{-1}, H/D kinetic isotope effect = 2.00$\pm$0.16). The resulting ketyl radical of AQDS follows fast deprotonation to the radical anion AQDS$^{\bullet-}$, that further reacts with oxygen (k = 1.2$\times 10^8$ M$^{-1}\cdot$s^{-1}), ultimately leading to the production of H_2O_2.

1. Introduction

The reconversion of abundant feedstocks into valuable chemicals is a hot and urgent topic embracing the fields of renewable energy and sustainable chemistry sectors. A significant example is provided by glycerol,[1] being a major by-product of soap manufacture and of biodiesel processing: as a result, current production of glycerol is larger than its demand, making it a cheap and easily available reactant.[2] Moreover, oxidation of glycerol may lead to several derivatives with appealing interest, such as dihydroxyacetone (DHA), glyceraldehyde, and C3 (glyceric GLA, tartronic, mesoxalic), C2 (glycolic GA, oxalic), C1 (formic FA) carboxylic acids.

In addition to thermocatalytic approaches targeting the oxidative valorization of glycerol, recent alternatives include plasma technologies,[3] pulse potential electrocatalysis,[4] and photocatalysis.[5–8] This latter approach is particularly attractive given the possibility of exploiting solar light as an inexhaustible source, in agreement with EU sustainable and development goals 7 (affordable and clean energy) and 13 (climate action). Photocatalysis has indeed collected a boost of reports in the last few years. Light-driven glycerol oxidation may take place in photoelectrochemical cells, taking advantage of n-type semiconductors as photoanodic materials,[9–11] eventually dye-sensitized and used in combination with an aminoxyl radical catalysts.[12] In these cases, primary oxidation products of glycerol are typically obtained (dihydroxyacetone,[10,11] glyceraldehyde[12] or glyceric acid),[9] and the anodic process is coupled to H_2 evolution developed at the cathode.[13] Beyond photoelectrochemical systems, wireless photocatalysis necessitates a simpler set-up. Wide bandgap materials[14] and in particular TiO_2 derivatives[15] have been considered in photocatalytic oxidation of glycerol. A recent report described decoration of TiO_2 with a AuPt alloys to achieve photocatalytic oxidation of glycerol to C3 products with good selectivity; most interestingly, this photocatalytic system was coupled to concomitant hydrogen peroxide generation from oxygen reduction.[16]

Among the different oxidation products deriving from glycerol, formic acid is a key C1 chemical that finds application in textile industry, agriculture, pharmacy, photoelectrochemical cells.[17]

Recent contributions of photoelectrochemical oxidation of glycerol to formic acid include a Ni covered Si photoanode reaching current densities up to 110 mA·cm^{-2} (using a solar simulator AM 1.5 at 10 sun intensity) obtaining formic acid as the main product, coupled to cathodic reduction of carbon dioxide.[18]

Concerning particulate photocatalysts, selective oxidation of glycerol to FA was achieved with TiO_2 photocatalyst, operating

E. Tacchi, G. Rossi, L. Đorđević, A. Sartorel
Department of Chemical Sciences
University of Padova
via Marzolo 1, Padova 35131, Italy
E-mail: luka.dordevic@unipd.it; andrea.sartorel@unipd.it
M. Natali
Department of Chemical Pharmaceutical and Agricultural Sciences (DOC-PAS)
University of Ferrara
Ferrara, Italy
E-mail: mirco.natali@unife.it

ADVANCED
SCIENCE NEWS

www.advancedsciencenews.com

ADVANCED
SUSTAINABLE
SYSTEMS

www.advsustainsys.com
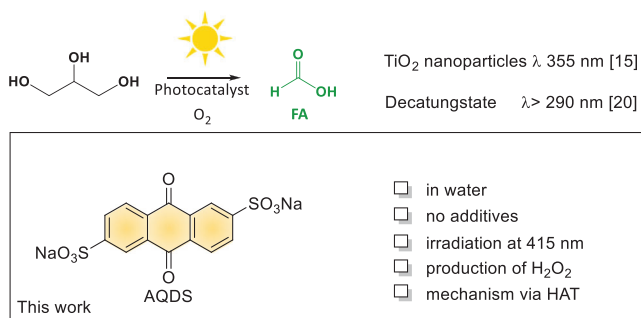
Scheme 1. Photochemical oxidation of glycerol by AQDS presented in this work.

in mixed acetonitrile/water and irradiating with 365 nm LED (5 W).[19]

Photocatalytic oxidation of glycerol to FA was also achieved in homogeneous solution, employing the sodium decatungstate ($Na_4W_{10}O_{32}$) photocatalyst under high energetic $\lambda > 290$ nm irradiation.[20] Surprisingly, organic photocatalysts have not been considered for light driven oxidation of glycerol, while recently quinone derivatives have been considered for glycerol acetylation and formation of Solketal.[21] A molecularly defined photocatalyst offers the opportunity to modulate the reactivity through structure reactivity correlation and mechanism analysis, and to expand the action spectrum of the photocatalyst in the visible region.

In this work, among various organic photocatalysts screened, we identify 9,10-anthraquinone-2,6-disulphonate disodium salt (AQDS) for promoting the aerobic photochemical oxidation of glycerol to formic acid (**Scheme 1**). Significant figures of merit of the system include: (i) operation in water with O_2 as the oxidant and without the need of additives; (ii) the use of blue light ($\lambda = 415$ nm); (iii) the concomitant formation of hydrogen peroxide from oxygen reduction; (iv) a mechanistic analysis combining electron paramagnetic resonance (EPR) spectroscopy, transient absorption spectroscopy (TAS), and DFT/TD-DFT calculations, suggesting a hydrogen atom abstraction from the triplet excited state of the photocatalyst as the primary step of glycerol oxidation.

2. Results and Discussion

2.1. Photochemical Glycerol Oxidation

In the case of glycerol oxidation, since products containing 1 to 3 carbon atoms can form, the yield $Y(P_j)\%$ and selectivity $S(P_j)\%$ of each product P_j are calculated according to Equations (1) and (2), that take into account the number of carbon atoms i present in the product P_j:[5]

$$Y\left(P_j\right)\% = \frac{mol(P_i) \times \left(\frac{i}{3}\right) \times 100}{mol(glycerol)_0} \quad (1)$$

$$S\left(P_j\right)\% = \frac{mol(P_i) \times \left(\frac{i}{3}\right) \times 100}{mol(glycerol)_0 - mol(glycerol)} \quad (2)$$

where $mol(P_j)$ are the mol of the product P_j, $mol(glycerol)_0$ are the initial mol of glycerol, $mol(glycerol)$ are the residual mol of glycerol and i is the number of carbon atoms in product P_j.

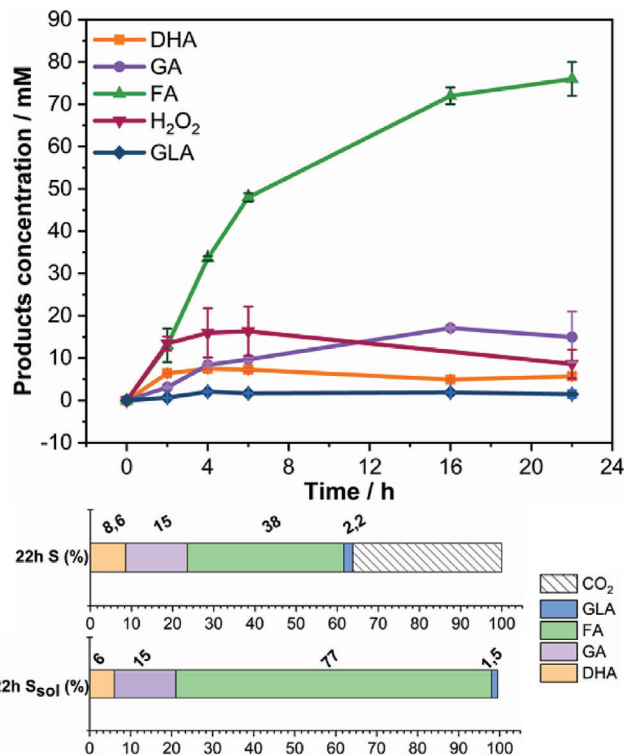**Figure 1.** Time profile of glycerol oxidation and selectivity under optimized conditions: [Glycerol] = 85 mM, [AQDS] = 5 mM, 415 nm LED light 200 mW·cm^{-2}, room temperature, under oxygen atmosphere. Selectivity S% and Solution Selectivity S$_{sol}$% are reported according to Equations (2) and (3).

In addition, we report also a solution selectivity for formic acid $S_{sol}(FA)\%$, taking into account the molar selectivity among the solution products:

$$S_{sol}\ (FA) = \frac{mol\ (FA)}{\sum_j mol\ (P_j)} \quad (3)$$

We started our investigation by evaluating several photocatalysts toward the aerobic oxidation of glycerol (85 mM in water, 2.5 mM photocatalyst, $\lambda_{irr} = 400$ nm with a Kessil lamp with a power density of 400 mW·cm^{-2}), in the absence of additives. This screening identified AQDS as the photocatalyst converting glycerol to FA, with yields up to 13% after 22 h. Alizarin Red S, Eosin Y, Erythrosin B, Phloxine B and [Ru(bpy)$_3$]Cl$_2$ (bpy = 2,2′-bipyridine) and blank experiments in the absence of photocatalyst led to null formation of oxidation products (Table S1, Supporting Information).

Optimization of the reaction conditions by operating under oxygen atmosphere and employing a panel of photoreactors (415 nm, power density of 200 mW·cm^{-2}) led to advanced 79% conversion of glycerol with AQDS (5 mM), obtaining 75 mM FA as the main product after 22 h, with GA, DHA and GLA being also detected (**Figure 1**).

Thus:

i) Y(FA)% approaches 30%, with selectivities S(FA) and S$_{sol}$(FA) of 38% and 77%, respectively; yields of DHA and

**ADVANCED
SCIENCE NEWS**

www.advancedsciencenews.com

**ADVANCED
SUSTAINABLE
SYSTEMS**

www.advsustainsys.com

of GA reach 7 and 12% respectively, with S(DHA) 8% and S(GA) 15%. A turnover number of 15 for AQDS referred to FA production is reached, while a turnover frequency of $1.68\ h^{-1}$ is calculated in the first 6 h of reaction, corresponding to a productivity of 4.1 mmol(FA) $g_{photocatalyst}^{-1}\cdot h^{-1}$. For the sake of comparison, a productivity of 5.31 mmol(FA) $g_{photocatalyst}^{-1}\cdot h^{-1}$ was obtained with TiO_2[15] at 355 nm. DHA and GA are obvious intermediates toward the production of FA, as confirmed by control experiments under analogous conditions starting with DHA or GA as the substrates and evidencing the formation of FA (23% and 16% yield starting from DHA and GA, respectively; also in this case, the reported yields consider the i factor as in eq. 1, see Table S2, Supporting Information). Monitoring the headspace in a separate experiment evidenced the evolution of CO_2,[15] accounting for the overall carbon balance (Table S2, Supporting Information).

ii) The quantum yield (QY) at 415 nm for FA production approaches 1.2% after 4 h.

iii) The reactivity of AQDS is significantly superior to the one of AQMS, for which the conversion of glycerol after 22 h irradiation was <5% (Table S2, Supporting Information).

iv) Most interestingly, hydrogen peroxide was detected in the reaction solution, reaching a maximum of 16±5 mM concentration after 6 h, while decreasing then to a plateau level of 9±3 mM up to 22 h. H_2O_2 is a high added-value product from dioxygen reduction in artificial photosynthesis strategies,[22–29] by combining photocatalysts with electron donors (indeed, < 1 mM H_2O_2 was detected in the absence of glycerol). A ca 30 mM concentration of H_2O_2 was recently reported with water-soluble perylene diimide photocatalysts using a broad range of sacrificial organic donors and operating in a wide pH range at 1 atm O_2.[30] Therefore, the 16±5 mM concentration obtained in this work under conditions optimized for glycerol oxidation represents a significant achievement. The depletion of H_2O_2 after reaching its maximum concentration can be explained by both its decomposition and its involvement in oxidation of DHA, GA and FA, as shown by control experiments (Table S3, Supporting Information).

2.2. Mechanistic Investigation Combining EPR, Transient Absorption Spectroscopy (TAS) and TD-DFT Calculations

The primary steps involved in the photocatalytic transformations were investigated by combining EPR, TAS experiments, and TD-DFT calculations.

In N_2-purged aqueous solution under the photochemical reaction conditions previously mentioned, the appearance of an orange color is noticed after few seconds of irradiation, with the color disappearing when exposing the solution to aerobic atmosphere.

To investigate the formation of paramagnetic products, electron paramagnetic resonance (EPR) spectroscopy was carried out. In situ irradiation (415 nm) of an aqueous AQDS (5 mM) solution in the presence of glycerol (85 mM in water) resulted in an EPR spectrum with a g-factor of 2.0212 that is consistent with the formation of the anthraquinone semiquinone radical anion
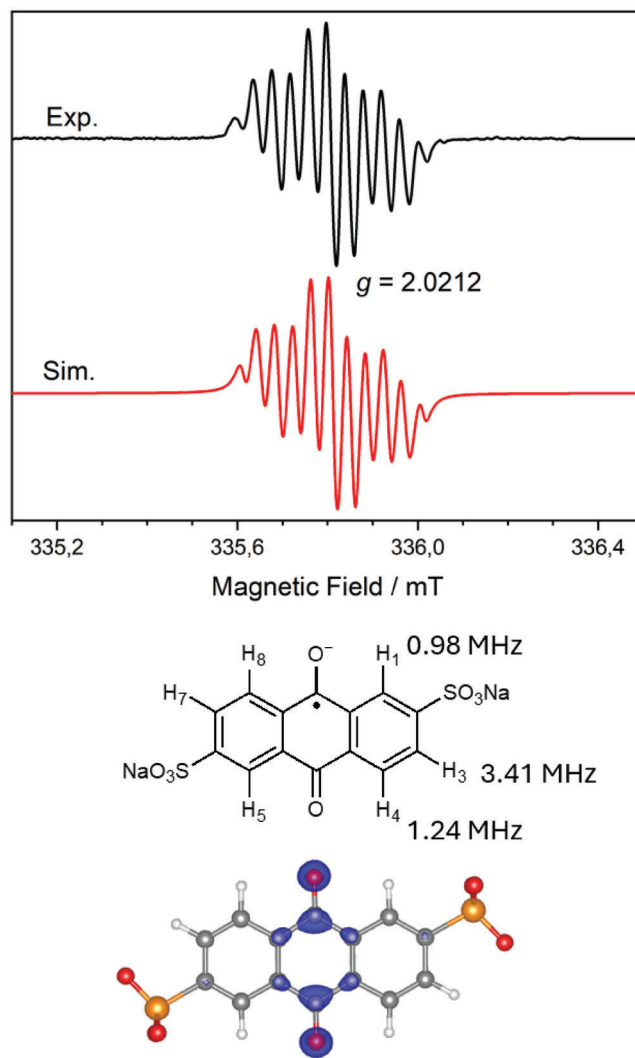

Figure 2. X-band EPR spectrum of photogenerated AQDS$^{\bullet-}$ at 298 K (85 mM glycerol, 5 mM AQDS in water; irradiation with blue LED at 415 nm, 200 mW·cm^{-2}). The multiplicity of the signal rules out the presence of the ketyl radical AQDSH (i.e., the conjugated acid of AQDS$^{\bullet-}$) that is characterized by different spectral features;[31] the absence of AQDSH in neutral aqueous solution is also consistent with a pKa of 3 for the AQDSH/AQDS$^{\bullet-}$ couple.[32] The chemical structure of AQDS$^{\bullet-}$ (only one resonance formula is shown) with the hyperfine coupling constants and the spin density of AQDS$^{\bullet-}$ (UB3LYP/TZVP level of theory) are also represented.

AQDS$^{\bullet-}$, **Figure 2**, whereas no EPR signal was detected in the absence of light. The simulated spectrum provides hyperfine coupling constants of $a^H_{H3,7} = 3.41$ MHz, $a^H_{H4,8} = 1.24$ MHz, and $a^H_{H1,5} = 0.98$ MHz (Figure 2), which are in agreement with a previous report.[31]

The spectral evidence of the AQDS$^{\bullet-}$ radical anion prompted us to investigate the associated dynamics by transient absorption spectroscopy. In N_2-purged aqueous solution, laser excitation at 355 nm of AQDS (0.16 mM) leads to the formation of absorption bands at 388, 480, and 640 nm which are characteristic of the triplet excited state ^{3}*AQDS,[33,34] formed in the sub-ns time scale via fast intersystem crossing from the singlet excited state. A

**ADVANCED
SCIENCE NEWS**

www.advancedsciencenews.com

**ADVANCED
SUSTAINABLE
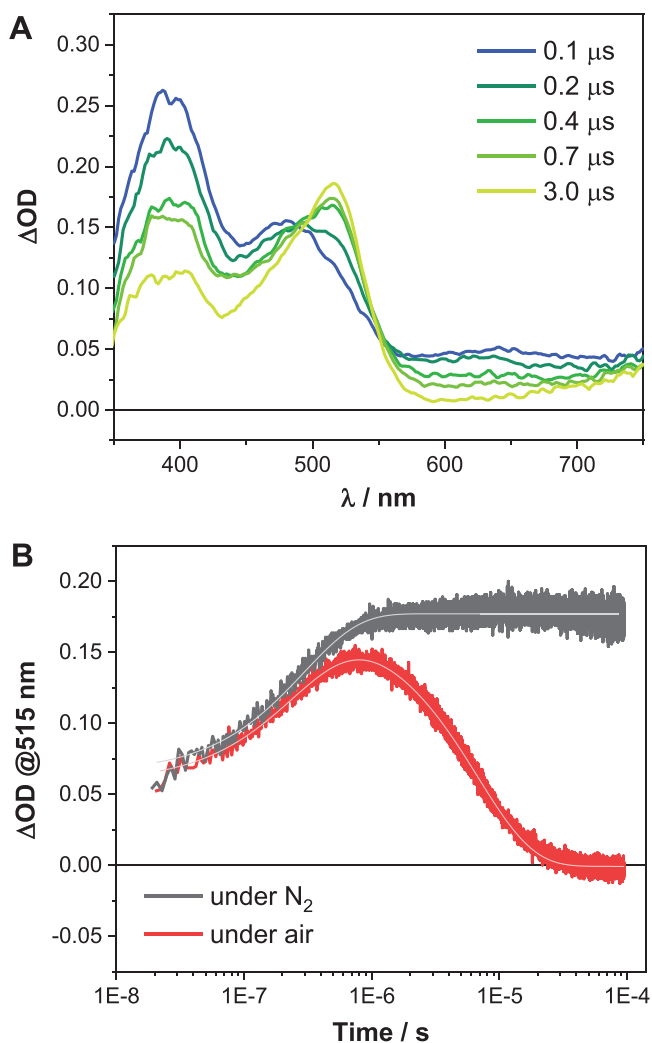SYSTEMS**

www.advsustainsys.com

Figure 3. A) Spectral evolution between 0.1-3 µs obtained by laser flash photolysis (excitation at 355 nm) of 0.16 mM AQDS in water in the presence of 0.2 M glycerol. Absorption bands at 388, 480, and 640 nm indicate prompt formation of the triplet excited state, while rising of the band at 515 nm indicates formation of the radical anion AQDS$^{\bullet-}$. B) Kinetic traces at 515 nm under N$_2$-saturated (black trace) and aerobic (red trace) conditions.

evolution (Figure 3A) points to a direct, smooth conversion of the triplet ^{3*}AQDS to the corresponding AQDS$^{\bullet-}$ anion in the presence of glycerol, in agreement with the previous EPR evidence.

Detailed kinetic analysis of the decay of the triplet ^{3*}AQDS at 400 nm and of the rise of the absorption of the AQDS$^{\bullet-}$ radical anion at 515 nm was subsequently performed within the concentration range 0–0.2 M glycerol (Figure S5, Supporting Information). Fitting of the kinetic traces allowed to estimate a bimolecular rate constant of $k = 1.22(\pm0.02)\times10^7$ M$^{-1}\cdot$s^{-1} for the reaction between ^{3*}AQDS and glycerol. From these data, an efficiency of $\eta = 47\%$ can be extracted for this primary photochemical process under the operative conditions employed in the photocatalysis experiments (remarkably, a bimolecular rate constant of $k = 1.02(\pm0.03)\times10^7$ M$^{-1}\cdot$s^{-1} and an efficiency of only $\eta = 14\%$ can be extrapolated for this primary photochemical process when employing the monosulfonate analog AQMS, in line with the lower reactivity of this latter under photocatalytic conditions, Figures S6–S8 and Table S1, Supporting Information). Interestingly, a H/D kinetic isotope effect (KIE) of 2.00±0.16 is observed when using glycerol-d_8 as a substrate (bimolecular rate constant of $k = 5.95(\pm0.15)\times10^6$ M$^{-1}\cdot$s^{-1}, see Figures S9–S12, Supporting Information). These results suggest that oxidation of glycerol by ^{3*}AQDS occurs through a hydrogen atom transfer (HAT, **Scheme** 2) with formation of the AQDSH$^\bullet$ ketyl radical[35–38] that further undergoes fast deprotonation to the experimentally observed anthraquinone radical anion AQDS$^{\bullet-}$. A fast deprotonation of AQDSH$^\bullet$ to AQDS$^{\bullet-}$ is expected considering the acidity of the ketyl radical AQDSH$^\bullet$, for which a pK_a of 3 was reported (photochemical identification and characterization of the ketyl radical AQDSH$^\bullet$ were indeed reported only in acidic aqueous conditions, pH 2).[32] Concerning the glycerol substrate, the hydrogen atom abstraction likely occurs at the more activated C2 position,[39,40] consistent with the formation of DHA as the primary oxidation product. Bimolecular rate constants in the range 10^6–10^7 M$^{-1}\cdot$s^{-1} (two to three orders of magnitude below the diffusion limit) are expected when C-H bonds are involved in a HAT process.[40]

The photochemical HAT is supported by the high hydrogen atom abstraction ability of ^{3*}AQDS, with an estimated Bond Dissociation Free Energy (BDFE) for the O-H bond in the ^{3*}AQDS/AQDSH$^\bullet$ couple of ca 111 kcal·mol^{-1} as derived from the Bordwell equation (equation 4):

$$BDFE\left(AQDSH^{\cdot}/^3*AQDS\right) = 1.37 \times pK_a\left(AQDSH^{\cdot}/AQDS^{\cdot-}\right)$$
$$+ 23.06 \times E_{red}\left(^3*AQDS/AQDS^{\cdot-}\right) + C_G \qquad (4)$$

where:

pK_a(AQDSH$^\bullet$/AQDS$^{\bullet-}$) = 3;[32]
E_{red}(^{3*}AQDS/AQDS$^{\bullet-}$) = E_{red}(AQDS/AQDS$^{\bullet-}$) + E^{00}(^{3*}AQDS) = 2.43 V, with:
E_{red}(AQDS/AQDS$^{\bullet-}$) = −0.30 V versus NHE
E^{00} (^{3*}AQDS) = 2.68 eV (61.8 kcal·mol^{-1})[41]

and

C_G = 52.2±0.6 kcal·mol^{-1}[42]

As expected, the transient signal of AQDS$^{\bullet-}$ (spectral trace at 515 nm in Figure 2B) is persistent under N$_2$ saturated at-

lifetime of 0.9 µs can be estimated for ^{3*}AQDS from the decay kinetics at 400 nm (Figure S1, Supporting Information), consistent with literature reports.[34] In the presence of glycerol, prompt formation of the triplet ^{3*}AQDS is still detected upon photoexcitation. However, the subsequent spectral evolution shows the generation within a few µs of a new transient signal with maximum at 515 nm (**Figure** 3A), clearly assigned to the AQDS$^{\bullet-}$ radical anion according to literature data,[34] but also through comparison with the absorption features observed by spectroelectrochemistry (Figures S2 and S3, Supporting Information; this analysis allows the determination of a redox potential for the AQDS/AQDS$^{\bullet-}$ couple of −0.30 V vs Normal Hydrogen Electrode, NHE) and considering the absorption spectrum calculated by TD-DFT (see Figure S4, Supporting Information). Furthermore, the observation of two isosbestic points at 489 and 551 nm in the spectral

**ADVANCED
SCIENCE NEWS**

www.advancedsciencenews.com

**ADVANCED
SUSTAINABLE
SYSTEMS**

www.advsustainsys.com

Scheme 2. Photochemical events involved in the light-driven oxidation of glycerol with AQDS.

mosphere within the timescale of 100 µs of the TAS experiment, while it decays in aerobic atmosphere due to re-oxidation of AQDS$^{\bullet-}$ to AQDS by O_2. Considering a solubility in H_2O of 1.2 mM for dioxygen,[43] a bimolecular rate constant of 1.2×10^8 $M^{-1} \cdot s^{-1}$ can be derived for this reaction.[34]

In this regard, single electron reduction of O_2 to the superoxide anion $O_2^{\bullet-}$ is expected, with $O_2^{\bullet-}$ being finally responsible for H_2O_2 production upon protonation (pK_a $HO_2^{\bullet}/O_2^{\bullet-}$ = 4.7) and subsequent dismutation.[44,45] We tried to confirm the formation of the superoxide anion $O_2^{\bullet-}$ by EPR spin trapping experiments employing 5,5-dimethyl-1-pyrroline *N*-oxide (DMPO). In particular, irradiation of an aqueous solution containing AQDS (5 mM), glycerol (85 mM) and DMPO (25 mM) leads to the raise of an EPR signal typical of the [DMPO-OH]$^{\cdot}$ spin adduct (Figure S13, Supporting Information),[46] as expected since [DMPO-OH]$^{\cdot}$ is known to rapidly form from the [DMPO-O$_2$]$^{\cdot-}$ spin-adduct in aqueous solution.[46] Therefore, the presence of the [DMPO-OH]$^{\cdot}$ signal can be definitely considered as an indirect proof of the photochemical generation of the superoxide anion. In this regard, the absence of EPR signals attributable to DMPO spin-adducts with carbon based radicals is not unexpected given the two orders of magnitude slower reactivity of DMPO with carbon radicals with respect to oxygen-based ones.[47]

Finally, a gradual conversion of AQDS along the photocatalytic irradiation conditions was observed by ^{1}H-NMR and UV-Vis spectroscopy (Figures S14 and S15, Supporting Information), with mass spectrometry analysis consistently supporting the formation of 4-sulfophthalate (Figure S16, Supporting Information). Strategies should thus be considered for preserving the integrity of the photocatalyst along operative conditions.

3. Conclusion and Perspectives

In this work, we have exploited an anthraquinone disulfonate organic photocatalyst to perform oxidation of glycerol to formic acid as the main product, coupled to production of hydrogen peroxide deriving from dioxygen reduction. The system operates in water in the absence of additives, exploiting dioxygen as the oxidant under visible light (λ = 415 nm), reaching a quantum yield for formic acid production of 1.2%. Investigation of the photochem-

ical mechanism supports a direct hydrogen atom transfer at the glycerol substrate operated by the triplet excited state ^{3*}AQDS.

We believe that this contribution provides an example of photocatalysis for smooth aerobic oxidation of organic raw materials in aqueous medium. This will help in the design and inspiration of novel photocatalytic systems toward solar reforming strategies,[8] that is, sunlight-driven transformation of waste substrates into valuable chemical products.

4. Experimental Section

Photooxidations were performed by using a homemade set-up, consisting of a photoreactor with 16 positions for 8.0 mL vials.[48] Typical conditions exploit 1 mL of a solution of photocatalyst and glycerol (85 mM) in mQ water introduced into the 8.0 mL vial; the reaction mixture was saturated with oxygen, and an oxygen headspace was maintained along the reaction by keeping a balloon connected to the headspace of the reactor; irradiation was performed from the bottom with blue LED (λ = 415 nm, power density of 200 mW·cm^{-2}; SemiLED C3535U-UNx1 U70 from LED-supply.com) under continuous stirring. Analysis of solution products was performed by HPLC and by ^{1}H-NMR using dimethylsulfone as internal standard. The quantum yield for FA production was determined from the ratio of FA mols and the photons absorbed, measured with a Thorlabs PM100USB power and energy meter with S120VC standard photodiode power sensor and ND10A-30A reflective filters. Analysis of the headspace for CO_2 detection and quantification was performed by gas chromatography using an Agilent Technologies 7890A GC system coupled to a TCD and to a 5975C mass spectrometer with triple-axis detector; the instrument is equipped with a HP-PLOTQ (15 m length, 0.32 mm OD, 20 µm film thickness) and a HP-MOLSIEVE (30 m length, 0.32 mm OD, 12 µm film thickness) columns put in series; only the first one has been used for analysis of CO_2.

Electron Paramagnetic Resonance (EPR) spectra were acquired on a Bruker ESR5000 operating at a microwave frequency of 9.4 GHz. 25 µL of solution samples were introduced into capillaries and sealed. The AQDS spectra were recorded using ESRStudio at room temperature with 0.6 mT microwave power, 0.02 mT modulation and 60 s sweep time. The AQDS degassed sample was irradiated in situ using 415 nm LED (same used for photooxidation experiments) for 60 s. For the spin trap experiments, 5,5-dimethyl-1-pyrroline *N*-oxide (25 mM DMPO, Merck code 92688) was introduced within the photocatalytic solution and irradiated for 30 s, before measuring the EPR signal (20 mW microwave power and 0.028 mT modulation, 60 s sweep time). The simulations were performed using the EasySpin software package (version 6.0.4).[49]

**ADVANCED
SCIENCE NEWS**

www.advancedsciencenews.com

**ADVANCED
SUSTAINABLE
SYSTEMS**

www.advsustainsys.com

DFT and TD-DFT calculations were performed with Gaussian 16 software[50] at the HPC facility of the Computational Chemistry Community of Padova (C3P). For TD-DFT and calculation of absorption spectrum the method UB3LYP/6-311G(d,p) was used, including a continuum solvation model for water using the integral equation formalism variant (IEF-PCM). The method UB3LYP/TZVP with the keyword prop = epr was used to calculate EPR properties and the spin density.[51]

Laser flash photolysis measurements were conducted using a custom laser spectrometer comprised of a Continuum Surelite II Nd:YAG laser (FWHM = 8 ns) with a frequency tripled option (355 nm) and an Applied Photophysics xenon light source. Laser excitation was provided at 90° with respect to the white light probe beam. Light transmitted by the sample was focused onto the entrance slit of a 300 mm focal length Acton SpectraPro 2300i triple grating, double exit monochromator equipped with a photomultiplier detector (Hamamatsu R3896) and a Princeton Instruments PI-MAX II gated intensified CCD camera. PMT signals (kinetic traces) were processed using a Teledyne LeCroy 604Zi (400 MHz, 20 GS/s) digital oscilloscope.

Cyclic voltammetries were registered with a BASi potentiostat, employing a glassy carbon electrode (diameter = 3 mm), a Pt counter electrode, and a Ag/AgCl reference electrode. Potentials were then converted to NHE according to E versus NHE = E versus Ag/AgCl +0.20 V.

Spectroelectrochemistry was conducted with a quartz cell equipped with a Pt gauze working electrode, a Pt counter electrode, and a Ag/AgCl reference electrode.[52]

Supporting Information

Supporting Information is available from the Wiley Online Library or from the author.

Acknowledgements

Conflict of Interest

The authors declare no conflict of interest.

Data Availability Statement

The data that support the findings of this study are available from the corresponding author upon reasonable request.

Keywords

[1] G. Dodekatos, S. Schünemann, H. Tüysüz, *ACS Catal.* **2018**, *8*, 6301.
[2] M. R. Karimi Estahbanati, M. Feilizadeh, F. Attar, M. C. Iliuta, *React. Chem. Eng.* **2021**, *6*, 197.
[3] S. Bang, R. Snoeckx, M. S. Cha, *ChemSusChem* **2024**, *17*, 202300925.
[4] W. Chen, L. Zhang, L. Xu, Y. He, H. Pang, S. Wang, Y. Zou, *Nat. Commun.* **2024**, *15*, 2420.
[5] H. H. Kuo, T. G. Vo, Y. J. Hsu, *J. Photochem. Photobiol. C Photochem. Rev.* **2024**, *58*, 100649.
[6] M. R. Karimi Estahbanati, M. Feilizadeh, F. Attar, M. C. Iliuta, *Ind. Eng. Chem. Res.* **2020**, *59*, 22330.
[7] Y. Liu, B. Zhang, D. Yan, X. Xiang, *Green Chem.* **2024**, *26*, 2505.
[8] S. Bhattacharjee, S. Linley, E. Reisner, *Nat. Rev. Chem.* **2024**, *8*, 87.
[9] Y. Xiao, M. Wang, D. Liu, J. Gao, J. Ding, H. Wang, H. Bin Yang, F. Li, M. Chen, Y. Xu, D. Xu, Y.-X. Zhang, S. Fang, X. Ao, J. Wang, C. Su, B. Liu, *Angew. Chem. Int. Ed.* **2024**, *63*, e202319685.
[10] H. Tateno, S. Y. Chen, Y. Miseki, T. Nakajima, T. Mochizuki, K. Sayama, *ACS. Sustain. Chem. Eng.* **2022**, *10*, 7586.
[11] D. Liu, J. C. Liu, W. Cai, J. Ma, H. Bin Yang, H. Xiao, J. Li, Y. Xiong, Y. Huang, B. Liu, *Nat. Commun.* **2019**, *10*, 1779.
[12] D. Bruggeman, A. Laoprte, R. J. Detz, S. Mathew, J. N. H. Reek, *Angew. Chem., Int. Ed.* **2022**, *61*, e202200175.
[13] Y. Miao, Z. Li, M. Shao, *ChemCatChem* **2024**, *16*, 202301321.
[14] P. Limpachanangkul, P. Nimmmanterdwong, L. Liu, M. Hunsom, K. Pruksathorn, P. Piumsomboon, B. Chalermsinsuwan, *Sci. Rep.* **2023**, *13*, 14936.
[15] M. Liu, H. Liu, N. Li, C. Zhang, J. Zhang, F. Wang, *ChemSusChem.* **2022**, *15*, e202201068.
[16] X. Liu, Y. Zou, J. Jiang, *Appl. Catal. B Environ.* **2024**, *350*, 123927.
[17] D. A. Bulushev, J. R. H. Ross, *ChemSusChem.* **2018**, *11*, 821.
[18] Á. Balog, E. Kecsenovity, G. F. Samu, J. He, D. Fekete, C. Janáky, *Nat. Catal.* **2024**, *7*, 522.
[19] L. Zani, M. Melchionna, T. Montini, P. Fornasiero, *J. Phys. Energy* **2021**, *3*, 031001.
[20] A. Molinari, A. Maldotti, A. Bratovcic, G. Magnacca, *Catal. Today* **2013**, *206*, 46.
[21] A. Matarín, L. González-Aguilera, M. L. Ferrer, M. Iglesias, E. M. Maya, *Sol. RRL* **2024**, *13*, 2400304.
[22] H. Hou, X. Zeng, X. Zhang, *Angew. Ed.* **2020**, *59*, 17356.
[23] B. C. Moon, B. Bayarkhuu, K. A. I. Zhang, D. K. Lee, J. Byun, *Energy Environ. Sci.* **2022**, *15*, 5082.
[24] Y. Isaka, Y. Kawase, Y. Kuwahara, K. Mori, H. Yamashita, *Angew. Chem., Int. Ed.* **2019**, *58*, 5402.
[25] Y. Ding, S. Maitra, D. A. Esteban, S. Bals, H. Vrielinck, T. Barakat, S. Roy, G. Van Tendeloo, J. Liu, Y. Li, A. Vlad, B.-L. Su, *Cell Rep. Phys. Sci.* **2022**, *3*, 100874.
[26] X. Li, X. Fan, H. Wang, Y. Chen, T. Yang, J. Ye, H. Huang, X. Zhang, Y. Liu, Y. Zhao, Z. Kang, *Appl. Catal. B Environ.* **2022**, *314*, 121499.
[27] J. Sun, Y. Wu, *Angew. Chem.* **2020**, *132*, 10996.
[28] Y. Zhang, X. Yang, H. Tang, D. Liang, J. Wu, D. Huang, *Green Chem.* **2020**, *22*, 22.
[29] H. B. Vibbert, C. Bendel, J. R. Norton, A. J. Moment, *ACS Sustain. Chem. Eng.* **2022**, *10*, 11106.
[30] M. Gryszel, T. Schlossarek, F. Wurthner, M. Natali, E. D. Glowacki, *ChemPhotoChem* **2023**, *7*, 202300070.
[31] J. Geimer, D. Beckert, *Chem. Phys. Lett.* **1998**, *288*, 449.
[32] Ž. Anusevičius, J. Šarlauskas, N. Čenas, *Arch. Biochem. Biophys.* **2002**, *404*, 254.
[33] I. Loeff, A. Trelnln, H. Linschltz, *J. Phys. Chem.* **1983**, *1569*, 2536.
[34] J. N. Moore, D. Phillips, N. Nakashima, K. Yoshihara, *J. Chem. Soc. Faraday Trans.* **1986**, *82*, 745.
[35] Á. Péter, S. Agasti, O. Knowles, E. Pye, D. J. Procter, *Chem. Soc. Rev.* **2021**, *50*, 5349.
[36] Y. Yan, G. Li, J. Ma, C. Wang, J. Xiao, D. Xue, *Green Chem.* **2023**, *25*, 4129.

**ADVANCED
SCIENCE NEWS**

www.advancedsciencenews.com

**ADVANCED
SUSTAINABLE
SYSTEMS**

www.advsustainsys.com

[37] J. Cervates-Gonzalez, D. A. Vosburg, S. E. Mora-Rodriguez, M. A. Vazquez, L. Gerardo Zepeda, C. Villegas Gomez, S. Lagunas-Rivera, *ChemCatChem* **2020**, *12*, 3811.

[38] J. Talvitie, I. Alanko, A. Lenarda, N. Durandin, N. Tkachenko, M. Nieger, G. W. Tagore, R. Chen, H. Crabtree, R. H. Brudvig, *ChemPhotoChem.* **2023**, *7*, e202300107.

[39] T. Newhouse, P. S. Baran, *Angew. Ed.* **2011**, *50*, 3362.

[40] M. Salamone, M. Galeotti, E. Romero-Montalvo, J. A. Van Santen, B. D. Groff, J. M. Mayer, G. A. Dilabio, M. Bietti, *J. Am. Chem. Soc.* **2021**, *143*, 11759.

[41] I. Loeff, J. Rabani, A. Treinin, H. Linschitz, *J. Am. Chem. Soc.* **1993**, *115*, 8933.

[42] R. G. Agarwal, S. C. Coste, B. D. Groff, A. M. Heuer, H. Noh, G. A. Parada, C. F. Wise, E. M. Nichols, J. J. Warren, J. M. Mayer, *Chem. Rev.* **2022**, *122*, 1.

[43] W. Xing, M. Yin, Q. Lv, H. Yang, C. Liu, J. Zhang, in *Rotating Electrode Methods Oxygen Reduction Electrocatalysts*, Elsevier, Amsterdam **2014**, pp. 1–31.

[44] D. T. Sawyer, J. S. Valentine, *Acc. Chem. Res.* **1981**, *14*, 393.

[45] G. V. Buxton, C. L. Greenstock, W. P. Helman, A. B. Ross, *J. Phys. Chem. Ref. Data* **1988**, *17*, 513.

[46] Z. MacHatova, Z. Barbieriková, P. Poliak, V. Jančovičová, V. Lukeš, V. Brezová, *Dyes Pig.* **2016**, *132*, 79.

[47] Z. Barbieriková, D. Dvoranová, V. Brezová, *Catal. Today* **2018**, *313*, 106.

[48] F. Arcudi, L. Ðorđević, N. Schweitzer, S. I. Stupp, E. A. Weiss, *Nat. Chem.* **2022**, *14*, 1007.

[49] S. Stoll, A. Schweiger, *J. Magn. Reson.* **2006**, *178*, 42.

[50] Gaussian 16, Revision C.01, M. J. Frisch, G. W. Truck, H. B. Schlegel, G. E. Scuseria, M. A. Robb, J. R. Cheeseman, G. Scalmani, V. Barone, G. A. Petersson, H. Nakatsuji, X. Li, M. Caricato, A. V. Marenich, J. Bloino, B. G. Janesko, R. Gomperts, B. Mennucci, H. P. Hratchian, J. V. Ortiz, A. F. Izmaylov, J. L. Sonnenberg, D. Williams-Young, F. Ding, F. Lipparini, F. Egidi, J. Goings, B. Peng, A. Petrone, Gaussian, Inc., Wallingford CT, **2016**.

[51] V. Barone, *Recent Advances in Density Functional Methods, Part I*, Ed.: D. P. Chong, World Scientific Publ. Co., Singapore **1996**.

[52] T. Chatterjee, E. Boutin, M. Robert, *Dalt. Trans.* **2020**, *49*, 4257.